EXFOLIATION SUSCEPTIBILITY OF ALUMINUM ALLOYS JOINED BY FRICTION STIR WELDING (FSW)

Mariana X. MILAGRE[1], Uyme Donatus[2], Caruline S.C. MACHADO[3], João Victor de Sousa ARAUJO[4], Vishnu Mogili[5], Antonello ASTARITA[6], Isolda COSTA[7]

[1]Instituto de Pesquisas Energéticas e Nucleares, CCTM, São Paulo, Brazil, marianamiagre@yahoo.com.br
[4]Instituto de Pesquisas Energéticas e Nucleares, CCTM, São Paulo, Brazil, uymedonatus@yahoo.com
[2]Instituto de Pesquisas Energéticas e Nucleares, CCTM, São Paulo, Brazil, carulinemachado@yahoo.com.br
[3]Instituto de Pesquisas Energéticas e Nucleares, CCTM, São Paulo, Brazil, joao-neutron@hotmail.com
[5]Laboratório Nacional de Nanotecnologia, LNNANO/CNPEM, Campinas, Brazil, vishnu.mogili@lnnano.cnpem.br
[6]University of Naples "Federico II", Napoli, Italy, antonello.astarita@unina.it
[7]Instituto de Pesquisas Energéticas e Nucleares, CCTM , São Paulo, Brazil, icosta@ipen.br

Abstract

In the present study, the exfoliation susceptibility of a commercial Al-Cu-Li alloy of the third generation, AA2098-T351, joined by FSW was investigated according to ASTM G34 standard practice and the results were compared with the results of the parent material. Susceptibility to exfoliation attack was classified by the depth of attack penetration. The cross-sections of the samples after test were observed by optical and scanning electron microscopy (SEM) to evaluate the penetration depth of corrosion attack. A comparison to conventional Al-Cu alloys (AA2024-T3/T351) was carried out and the results showed that the Al-Cu-Li alloy tested (AA2098-T351) was more susceptible to exfoliation. Besides, exfoliation susceptibility varied with each welded zone and the active zones remained active for long periods of time after removal from the test solution when the attack continuously propagated in the corrosion front.

Key-words: exfoliation, aluminum–lithium alloys, friction stir welding.

Introduction

The friction stir welding (FSW) process was developed in the 90's as an alternative process for welding materials that are hardly welded by conventional processes. The major characteristic of this process is that welding occurs in the solid state. The heat source for joining the materials is provided by the rotation and transverse movements of a pin generating sufficient heat for softening and welding. This process showed advantages for welding of Al-alloys and has been employed in the aircraft industry [1–3].

Despite the good mechanical properties of the joints generated by FSW process, it causes changes in the material microstructure. The different thermal and mechanical effects along the welded joint allow the classification of the zones into three main zones affected by welding. The stir zone (SZ) is the zone where the mixture of the joined materials occurs and high temperatures are reached, consequently, recrystallization and phase dissolution are observed. The thermomechanically affected zone (TMAZ) is the zone where the effect of tool rotation, the high temperatures and the enclosure caused by the shoulder lead to grain deformation, phase dissolution and coarsening. In the heat affected zone (HAZ) the temperatures reached are not sufficient to change the grain shape relative to the base metal (BM) but dissolution and phase coarsening has been reported [4–8].

Aluminum alloys are susceptible to many types of localized corrosion, such as intergranular corrosion (IGC) and stress corrosion cracking (SCC) [9–13]. Exfoliation is a kind of intergranular corrosion where the stresses caused by the corrosion products formed in the grain boundaries lead to separation of grains [14]. The elongated grain shape is an important microstructural feature for this form of corrosion [14,15]. According to the literature [15], galvanic coupling between the precipitates and the precipitate free zones (PFZ) are also requisites for this type of corrosion attack. According to Robinson [15], heat treatment conditions influence exfoliation corrosion.

Aluminum-copper-lithium (Al-Cu-Li) alloys were developed as potential substitutes for the conventional aluminum alloys of the 2XXX series, for example, AA2024 alloys [16–19]. The exfoliation behavior of AA2024 was reported by many authors [20–23]. Keddam *et al*. [20] used electrochemical techniques to report the exfoliation susceptibility of AA2024-T351 in EXCO solution. The susceptibility to exfoliation corrosion of AA2024-T3 was studied by Liu *et al* [14] using the foil penetration. The effect of the different artificial ageing conditions to exfoliation susceptibility of AA2024 was reported by Alexopoulos [24]. Kamoutsi *et al*. [22] showed that corrosion attack starts with pitting that develops into intergranular attack and exfoliation. Posada *et al*. [23] cited chemical differences between the boundaries of high angles and those parallel to the plate plane.. They also suggested that the anodic sites play less significant role in the propagation of exfoliation than the corrosion products which forms between the elongated grain boundaries.

In a similar manner to the conventional alloys of the 2XXX series, Al-Cu-Li alloys are susceptible to exfoliation corrosion [25]. Giummarra *et al* .[25] observed that the 2199 Al-Cu-Li alloy has significantly better exfoliation corrosion resistance compared to the AA2024. According to Liang *et al.* [26] intergranular corrosion and exfoliation corrosion of an Al-Cu-Li alloy is caused by anodic dissolution of T1 phase and the precipitate-free zone (PFZ). Kelly and Robinson [27] also showed that for Al-Cu-Li alloys, the grain shape and heat treatment conditions are factors that influence the exfoliation susceptibility of this class of materials.

It is well known that FSW process affects the corrosion behavior of Al-alloys [28,29,38,30–37]. However, despite the large information about the exfoliation corrosion susceptibility of Al alloys, the effect of the FSW process on the exfoliation susceptibility of Al-Cu-Li alloys is still rare. Chen *et al.* [29] reported that the HAZ of an Al-Cu-Li alloy is susceptible to exfoliation and attributed this to the high temperatures reached in HAZ promoting the precipitation of T2 phase at the grain boundaries. According to Chen *et al.* [29] the T2 phase is responsible for the severe intergranular exfoliation corrosion observed. In the present work, the exfoliation susceptibility of the AA2098-T351 was investigated in EXCO solution and compared with that of the AA2024-T3 and AA2024-T351 alloys. The exfoliation susceptibility of the AA2098-T351 alloy welded by FSW was also evaluated and the results were compared with that of the parent metal.

Experimental

The chemical composition of the alloys used in this study is shown in Table 1.

Table 1 - Chemical composition (wt%) obtained by Inductively Coupled Plasma-Atomic Emission Spectroscopy (ICP-AES) of the Al alloys used.

Al-alloy\Element	Al	Cu	Li	Mg	Ag	Zr	Fe	Si	Zn	Mn
AA2024-T3	93.5	4.2	-	1.6	-	-	0.20	0.01	0.02	0.4
AA2024-T351	93.2	4.5	-	1.4	-	-	0.12	0.03	0.02	0.6
AA2098-T351	94.5	3.4	1.0	0.3	0.3	0.4	0.04	0.05	0.02	0.003

FSW was performed using a rotational speed of 700 rpm, a transverse speed of 300 mm/min and load in the range of 8 kN – 15 kN. A H13 steel tool with a 16 mm diameter shoulder and adjustable pin, 3.2 mm of length in accord with the plate thickness, was used. Thermocouples were attached underneath the plate, at distances of 6, 9 mm and 12 mm from the center of the joint to obtain the thermal profile and to perform simulations referring to the temperature profile. Thermal simulations were performed using the finite element COMSOL v5.2 software. The physical phenomena in welding, such as heat transfer by conduction and radiation, were considered. The welding model counted 86009 elements. The thermal conductivity and specific heat of the AA2024 alloy were adopted as reference in the COMSOL database, since the data for the alloy used in this work are not yet available. Measurements obtained by the thermocouples were used as input data for calibration of the thermomechanical model. Exfoliation corrosion susceptibility test was performed according to the ASTM G34 practice. Prior to immersion, the specimen surface was cleaned by immersion for 10 min in alcohol isopropyl using an ultrasonic bath. After surface preparation, specimens were immersed for 48h in the test solution composed of 4.0 mol L^{-1} of NaCl, 0.5 mol L^{-1} of KNO_3 and 0.1 mol L^{-1} of HNO_3. Optical and scanning electron microscopy (SEM) images of surface and cross section were acquired using a Leica model DMLM and a Hitachi TM 3000 microscope with an incident beam of 15 keV. The surface was prepared by metallographic techniques, specifically mechanical polishing with silica carbide abrasives (#320, #550, #800, #1200, #4000) and diamond suspension of 3 μm and 1 μm. An etching solution composed by 25% HNO_3 and 3% HF in deionized H_2O was used for revealing of microstructural features. Monitoring of exfoliation evolution after removal from test solution was carried out at different times of samples exposure

to the room ambient. Samples of AA2024- T351, AA2024-T3 and AA2098-T351 plates were used. The welded sample was cropped in 3 parts as shown in Figure 1.

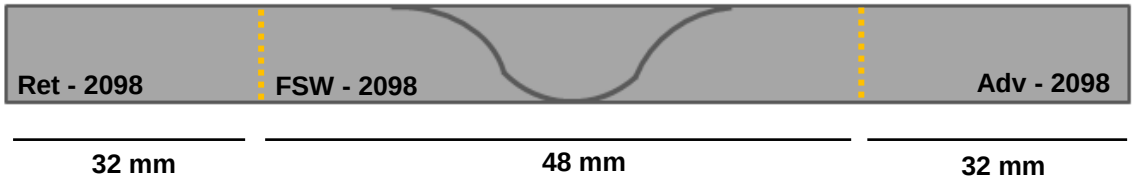

Figure. 1 – Schema of welded samples crop used in the exfoliation test according to ASTM G34.

Results and discussion

Macroscopic observations of the samples during exposure to EXCO test solution showed high reactivity of the samples to the tested media, mainly the ones with T351 temper, by the bubbles formation, Figure 2.

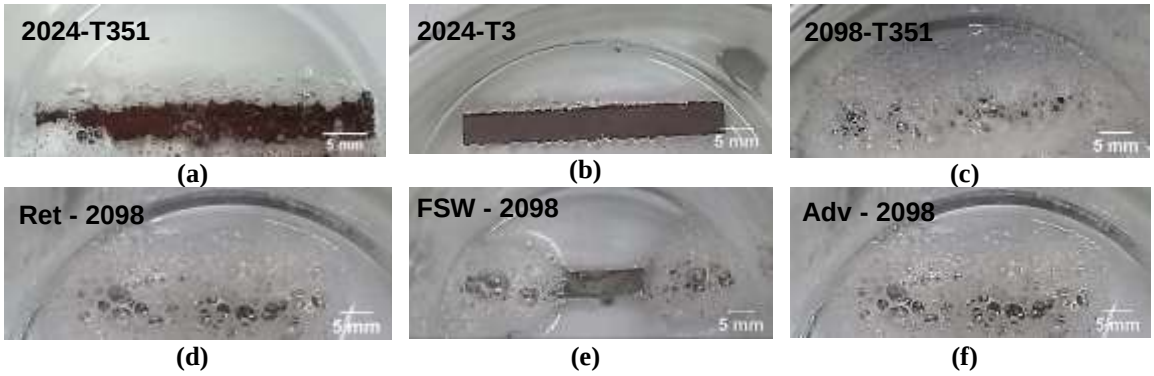

Figure 2 – Samples during the immersion test in EXCO solution. (a) AA2024-T351; (b) AA2024-T3; (c) AA2098-T351; (d) Welded sample (retreating side); (f) Welded sample; (d) Welded sample (retreating side.

Stretching largely increased the reactivity of the AA2024 alloy, as observed in Figure 2a and 2b, and the AA2098-T351 alloy showed the highest susceptibility to corrosion attack in the EXCO solution. As for the welded samples, Figure 2 (d)-((f), the welding joint (SZ and TMAZ) was the most resistant to corrosion attack in EXCO and no bubbles were observed on this zone. On the other hand, the HAZ and parent metal (PM) of the AA2098-T851 alloy, either in the advancing or retreating sides, were highly susceptible to corrosion attack. After 48h of exposure to EXCO, the samples were removed from this solution rinsed and then left to dry at room temperature. Figure 3 shows the surface of the tested samples after 48h of test.

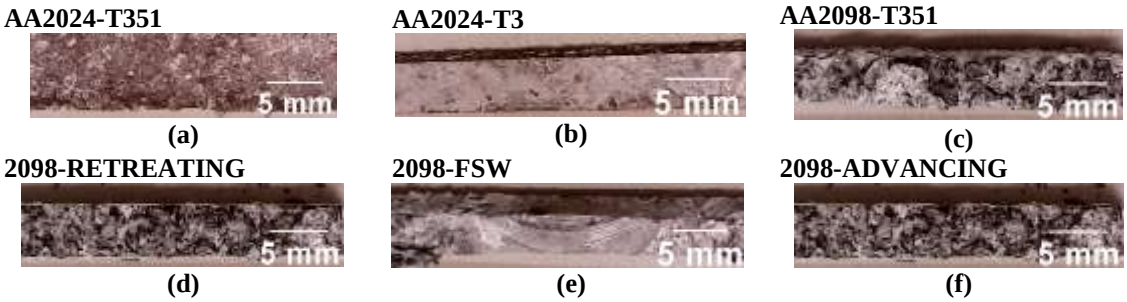

Figure 3 – Surface of samples after 48h of immersion in EXCO solution. (a) AA2024-T351; (b) AA2024-T3; (c) AA2098-T351; (d) AA2098-T351 (retreating side); (e) AA2098-T351 welded by FSW; (f) AA2098-T351 (advancing side).

The effect of stretching on exfoliation susceptibility of Al-alloys is supported by the macroscopic observation of the Al-alloys surfaces after 48h of immersion in EXCO solution, Figure 3a and 3b. The AA2024-T3 showed small pits distributed over the surface, however, in the AA2024-T351, some entire grains were completely attacked. Grains separation was observed in the AA2024-T351. Comparatively to the tested alloys, the AA2098-T351 showed the highest susceptibility to exfoliation, Figure 3c. Besides, the various zones in the welded sample presented different corrosion resistance. The cropped regions, Figure 3d and 3f, showed the same surface aspect of the parent metal (PM), Figure 3c. However the welding joint (ZTMA and SZ), Figure 3e, showed the highest resistance to exfoliation. It must be highlighted that a region in the HAZ, the nearest to the welded joint (yellow dashed lines) also showed high resistance to exfoliation.

The influence of grain shape on exfoliation susceptibility of Al-alloys has been previously reported [15,27,39,40]. Figure 4 shows the different grains morphologies for the samples analyzed.

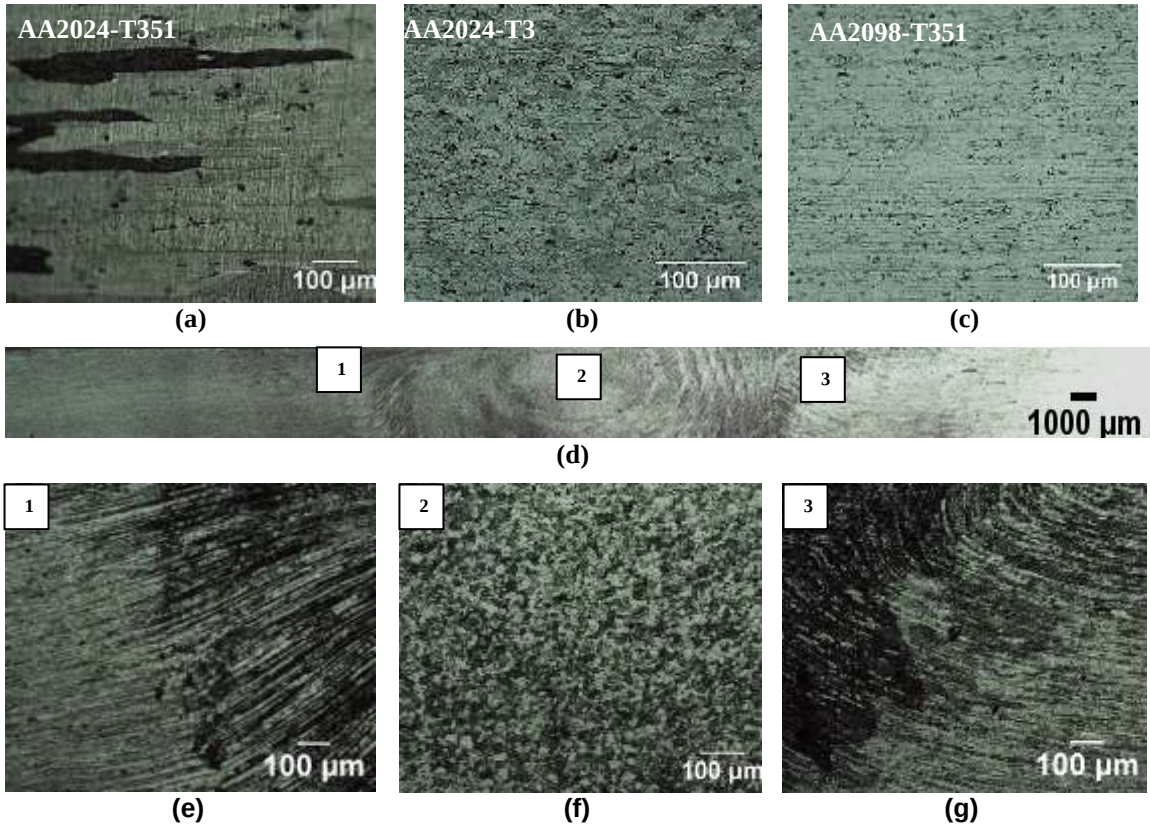

Figure 4 – Macrographs of the cross section of samples exposed to exfoliation test (ASTM G34 practice).

The tested samples presented different grain shapes. The AA2024-T351showed elongated grains, Figure 4a, whereas the AA2024-T3, presented much smaller grains with different shapes, Figure 4b. Besides, at the welding joint, specifically in the SZ, equiaxial grains were observed, Figure 4f, whereas in the other welded zones, elongated grains were seen (Figure 4e and 4g). Elongated grains are also characteristics of the parent metal (PM). In the SZ, the high temperatures reached lead to recrystallization of the alloy [4,8,41].

Optical micrographs of the cross section of samples exposed for 48h to EXCO solution were also obtained. Figure 5 compares the effect of tempers T3 and T351 on the exfoliation susceptibility of AA2024.

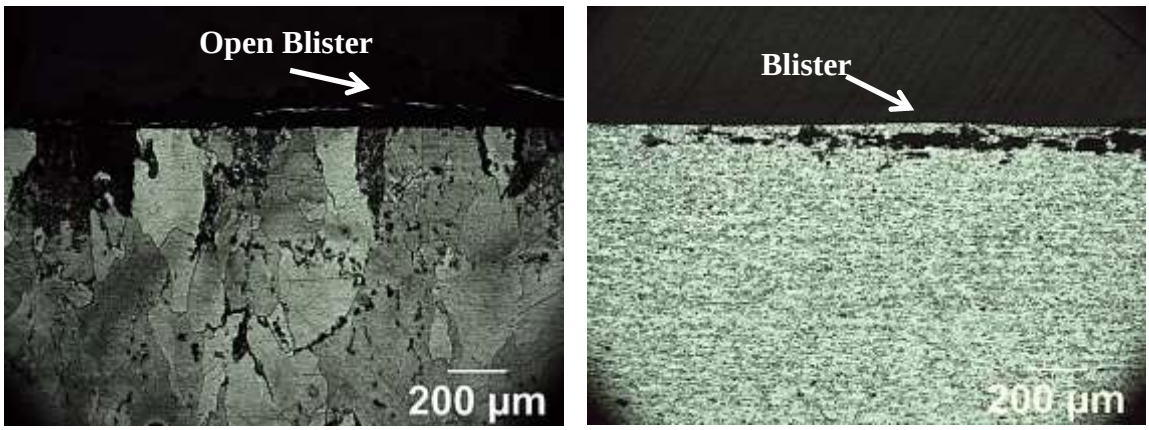

Figure 5 – Micrographs of AA2024 with different tempers and tested for 48h of exposure to EXCO solution; (a) T351; (b) T3.

According to Figure 5 the AA2024-T351 showed more susceptibility to exfoliation than AA2024-T3. For both alloys the blisters formations were observed, however the major amount of corrosion products in AA2024-T351 was responsible for the opening of the blister. The temper condition T351 comprise an step of pre-strain which is known for increase the amount of the precipitates. The main precipitate responsible for increase the strength in the Al-Cu alloys is the S phase (Al_2CuMg) which is anodic in relation to the matrix. According to Robinson [15] , the first stage of exfoliation corrosion is the intergranular attack which occurs as result of local cells. The intergranular corrosion (IGC) mechanism in AA2024 alloys caused by the development of precipitation free zones (PFZ) along the grain boundaries. These sites are preferential regions of attack, but S phase particles at the grain boundaries are also attacked [42]. S phase dissolution leads to Cu deposition in the grain boundaries vicinities protecting these sites and the corrosion attack propagates in the grain boundaires [42]. Zhou *et al*.[43] related IGC with the attack of clusters of S-phase particles that resulted in a deep corrosion front and when this encounters a grain boundary, the attack develops preferentially through the grain boundaries. For Hughes *et al.* [44] copper-rich precipitates ($CuAl_2$) can be formed at grain boundaries and copper-depleted regions can develop adjacent to these boundaries, which are anodic with respect to copper-rich grain boundaries and the alloy matrix. Also, S phase particles (typically <100 nm) anodic relatively to the adjacent matrix, are preferentially precipitated at grain boundaries, resulting in their preferential dissolution. Luo *et al.* [45] cited that grains with high dislocation densities are more susceptible to preferential attack in the grain boundaries. The effect of temper condition was also reported by Zhang *et al.* [42] . In their study, the T351 temper favored precipitation of fine intermetallic S phase particles at the grain boundaries leaving a matrix impoverished in copper and forming copper-depleted zones along the grain/subgrain boundaries that favored IGC propagation.

Higher exfoliation susceptibility was presented by the AA2098-T351 in relation to AA2024, in both temper conditions. In the AA2098-T351, exfoliation susceptibilities varied according to the zone tested. Figure 6 shows micrographs of the BM and the welded sample after 48h of exposure to EXCO solution.

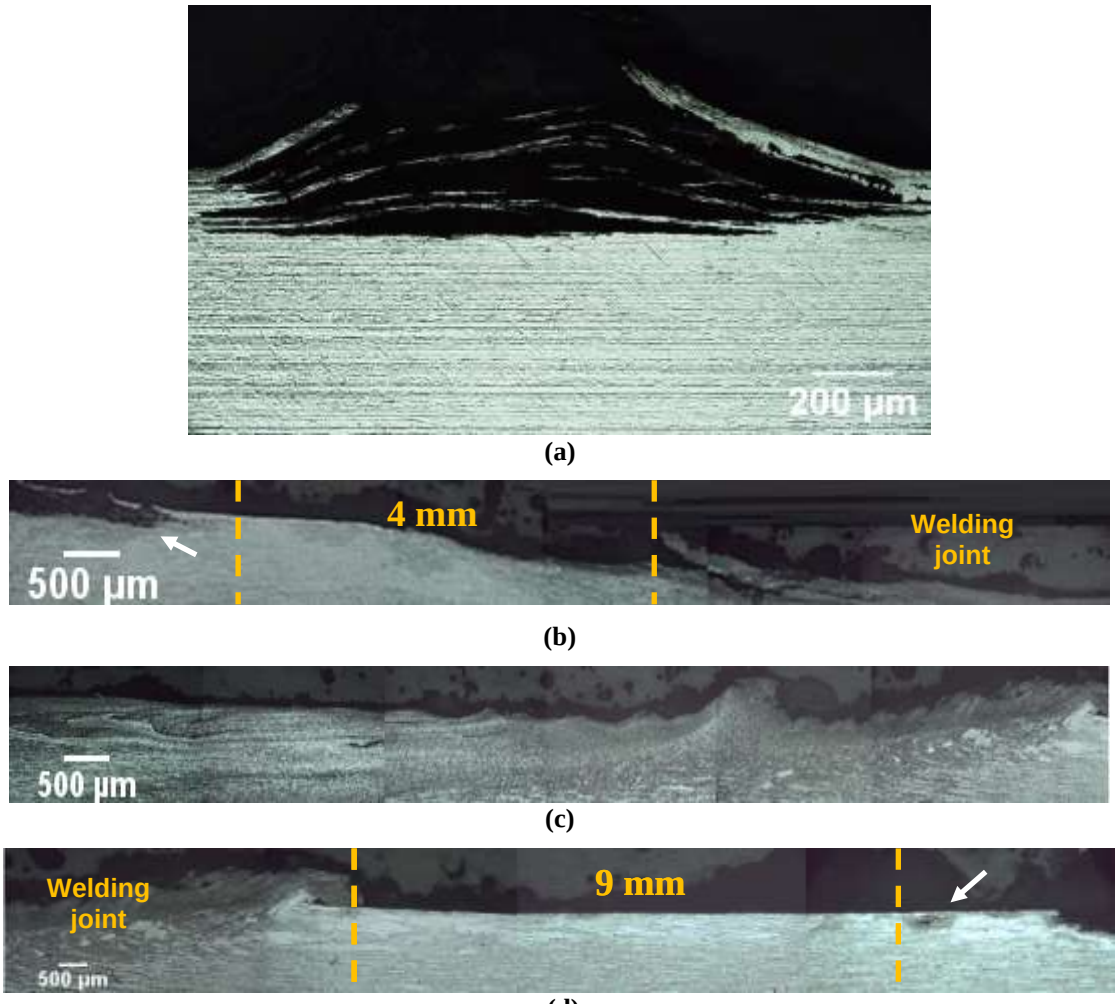

Figure 6 – Optical micrographs of AA2098-T351 after 48h exposure to EXCO solution. (a) PM; (b) AA2098 sample with FSW (Retreating side); (c) Welding joint; (c) AA2098 with FSW (Advancing side).

Intergranular corrosion of Al-Cu-Li alloys has been described by many authors and often associated to Cu depleted zones and the T1 microgalvanic coupling with the PFZ [26,46–48]. Kertz *et al*. [49] showed that localized corrosion along the grain boundaries is related with the T1 precipitation at high angle boundaries. According to Li *et al* [13] the susceptibility of Al alloy to exfoliation is dependent on precipitates size; heat treatments that promote precipitation of large phases decrease resistance to exfoliation.

Figure 6b,c and d showed different parts of the FSW-2098 samples, as the results showed, exfoliation was not observed in the welding joint (SZ and ZTMA). This behavior is due to the high temperatures reached in these zones that allow recrystallization and phase dissolution, Figure 7. Besides, in the HAZ nearest to the weld joint, no susceptibility to exfoliation was observed, despite the fact that this region presented grains with similar aspect to those of the BM, Figure 6a. The extension of this region was larger for the advancing side, Figure 6d, than for the retreating one, Figure 6b. The white arrows in Figure 6 (b) and (d) indicate the sites where exfoliation corrosion was clearly seen.

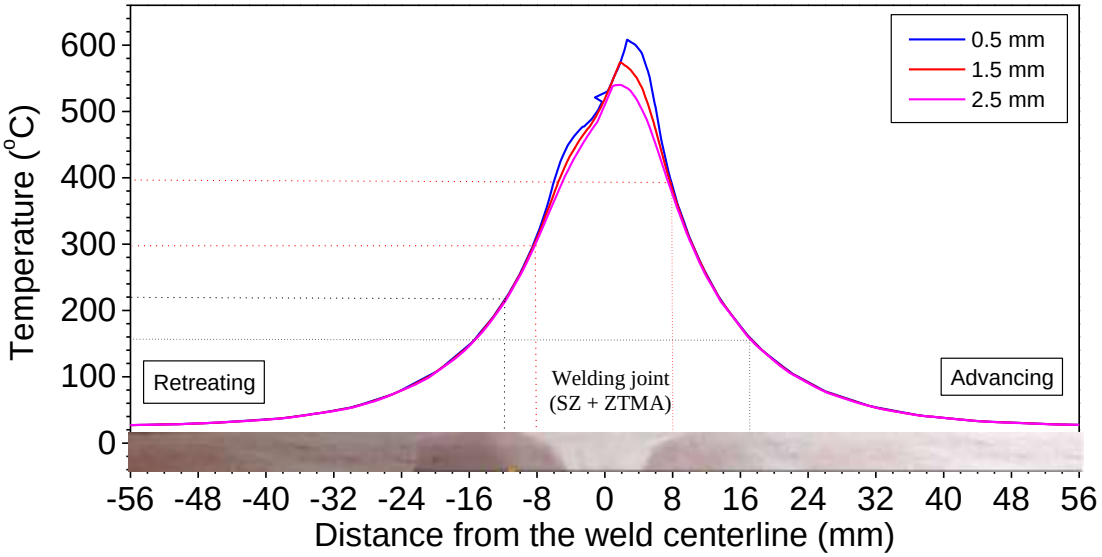

Figure 7 - Thermal simulation profile at different thickness distances.

Low temperatures can also affect the microstructure of Al alloys [50–52] According to Chen and Bhat [53], the T1 phase is affected by temperatures as low as around 137 °C. The results presented showed that resistance to exfoliation starts at 12 mm and 17 mm from the weld centerline, for retreating and advancing sides, respectively. At these positions, the temperatures reached during the welding process were about 210 – 160 °C (dashed lines), Figure 7. For more than 5 mm, approximately, the grain shapes are elongated as the metal base, however no exfoliation was observed. Thus, the behavior observed in Figure 6, is related to T1 phase dissolution that is also responsible for microgalvanic coupling with the PFZ zones promoting intergranular corrosion and, consequently, exfoliation. The effect of the temperatures reached during FSW in each zone on T1 phase distribution and morphology were investigated by TEM analysis in our previously work [54].

An interesting behavior was observed in the different samples cropped from the welded AA2098-T351 and the BM tested for 48h of exposure to EXCO solution followed by their removal from this solution, drying, and monitoring of the corrosion front advance with time of exposure to the environment at room temperature. It was seen that in the tested samples corrosion remained active for long periods of time, as Figure 8 shows.

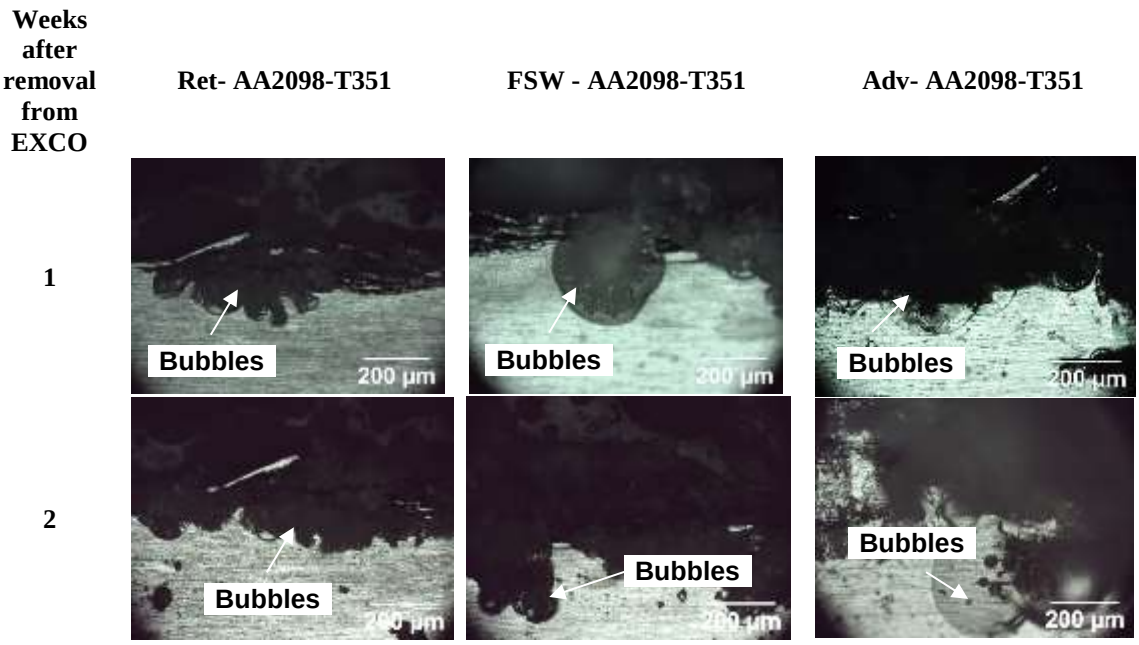

Figure 8 – Actives sites that remained in welded samples tested by exposure for 48h in EXCO solution. Withe arrows point to bubbles.

This behavior indicates that the susceptibility to corrosion of the AA2098-T351 alloy welded sample The continuous observation of hydrogen bubbles and corrosion products formation on the AA2098-T351 alloy surface even after weeks of removal from the electrolyte means that once exfoliation is initiated, the driving force for its propagation is high. There is enhanced dissolution and hydrolysis due to the presence of Li in the matrix and in the high volume fraction of the highly active T1 phase. This results in more significantly pH decrease at the corrosion front of the AA2098-T35, and together with the ingress of chloride ions (for electro-neutrality, especially as the active corrosion front is deprived of oxygen due to the covering from corrosion products), the attack is much more autocatalytic.

Conclusions

The susceptibility to exfoliation attack of the Al- alloys was evaluated. The AA2024-T3 showed higher resistance to exfoliation than the AA2024-T351one. The AA2098-T351 showed the highest susceptibility to exfoliation compared to the AA2024 in both tempers tested. The sample welded by FSW showed different susceptibility to exfoliation according to the zones affected by welding. The welding joint showed higher resistance to exfoliation than the parent metal. Resistance to exfoliation was also found in the HAZ nearer to the weld centerline. The widths of HAZ with high resistance to exfoliation varied between the advancing and retreating side. Monitoring of the samples tested in EXCO after removal from this solution with time of exposure to the laboratory environment showed that corrosion activity remained for long periods of time after their removal form the solution and drying.

Acknowlegments

The authors acknowledge CAPES (Capes/Cofecub No 806-14) and FAPESP (2013/13235-6) for financial support for this work and to CAPES for the grants of M.X. Milagre (99999.000332/2016-00), C.S.C. Machado (99999.000400/2016-05) and FAPESP for the grants of U. Donatus (Proc.2017/03095-3). Acknowledgements are also due to Dr. Maysa Terada, Rafael Giorgão and Victor Ferrinho Pereira from Brazilian Nanotechnology National Laboratory (LNNano) for carried out the welding of AA2098-T351 plate.

References

1. P. L. Threadgill, A. J. Leonard, H. R. Shercliff, and P. J. Withers, *Int. Mater. Rev.*, **54**, 49–93 (2009).
2. R. Nandan, T. Debroy, and H. K. D. H. Bhadeshia, *Prog. Mater. Sci.*, **53**, 980–1023 (2008).
3. R. S. Mishra and Z. Y. Ma, *Mater. Sci. Eng. R Reports*, **50**, 1–78 (2005).
4. R. W. Fonda and J. F. Bingert, *Metall. Mater. Trans. A Phys. Metall. Mater. Sci.*, **37**, 3593–3604 (2006).
5. A. K. Shukla and W. A. Baeslack, *Sci. Technol. Weld. Join.*, **14**, 376–387 (2009).
6. A. K. Shukla and W. A. Baeslack, *Scr. Mater.*, **56**, 513–516 (2007).
7. J. C. Rao et al., *Adv. Eng. Mater.*, **12**, 298–303 (2010).
8. P. Cavaliere, M. Cabibbo, F. Panella, and A. Squillace, *Mater. Des.*, **30**, 3622–3631 (2009).
9. A. C. U. RAO, V. VASU, M. GOVINDARAJU, and K. V. S. SRINADH, *Trans. Nonferrous Met. Soc. China (English Ed.*, **26**, 1447–1471 (2016).
10. T. S. Huang and G. S. Frankel, *Corros. Sci.*, **49**, 858–876 (2007).
11. S. P. Knight, M. Salagaras, and A. R. Trueman, *Corros. Sci.*, **53**, 727–734 (2011).
12. W. Zhang, S. Ruan, D. A. Wolfe, and G. S. Frankel, *Corros. Sci.*, **45**, 353–370 (2003).
13. H. ying LI, Y. TANG, Z. de ZENG, and F. ZHENG, *Trans. Nonferrous Met. Soc. China*, **18**, 778–783 (2008).
14. X. Liu, G. S. Frankel, B. Zoofan, and S. I. Rokhlin, *Corros. Sci.*, **46**, 405–425 (2004).
15. M. J. Robinson, *Corros. Sci.*, **22**, 775–790 (1982).
16. P. Lequeu, K. P. Smith, and A. Daniélou, *J. Mater. Eng. Perform.*, **19**, 841–847 (2010).
17. T. Warner, *Mater. Sci. Forum*, **519**–**521**, 1271–1278 (2006).
18. Y. Ma et al., *Electrochim. Acta*, **80**, 148–159 (2012).
19. J. A. Moreto, C. E. B. Marino, W. W. Bose Filho, L. A. Rocha, and J. C. S. Fernandes, *Corros. Sci.*, **84**, 30–41 (2014).
20. Keddam M., C. Kuntz, H. Takenouti, D. Schuster, and D. Zuili, *Electrochim. Acta*, **42**, 87–97 (1997).
21. N. D. Alexopoulos, Z. Velonaki, C. I. Stergiou, and S. K. Kourkoulis, *Corros. Sci.*, **102**, 413–424 (2016).
22. H. Kamoutsi, G. N. Haidemenopoulos, V. Bontozoglou, and S. Pantelakis, *Corros. Sci.*, **48**, 1209–1224 (2006).
23. M. Posada et al., *Mater. Charact.*, **38**, 259–272 (1997).
24. N. D. Alexopoulos, *Mater. Sci. Eng. A*, **520**, 40–48 (2009).
25. C. Giummarra, B. Thomas, and R. Rioja, *Proc. Light Met. Technol. Conf. 2007*

(2007).
26. L. Wenjie et al., *Rare Met.*, **27**, 146–152 (2008).
27. D. J. Kelly and M. J. Robinson, *Corros. Sci.*, **49**, 787–795 (1993).
28. M. Jariyaboon et al., *Corros. Sci.*, **49**, 877–909 (2007).
29. M. H. Chen, R. Y. Hwang, and C. P. Chou, **4**, 21–27 (1999).
30. G. T. andV. G. F. Zucchi, **859**, 853–859 (2001).
31. V. Proton et al., *Corros. Sci.*, **73**, 130–142 (2013).
32. C. S. Paglia and R. G. Buchheit, *Scr. Mater.*, **58**, 383–387 (2008).
33. J. C. B. Bertoncello, S. M. Manhabosco, and L. F. P. Dick, *Corros. Sci.*, **94**, 359–367 (2015).
34. J. Corral, E. a Trillo, Y. Li, and L. E. Murr, *J. Mater. Sci. Lett.*, 2117–2122 (2000).
35. E. Bousquet, A. Poulon-Quintin, M. Puiggali, O. Devos, and M. Touzet, *Corros. Sci.*, **53**, 3026–3034 (2011).
36. A. Davoodi, Z. Esfahani, and M. Sarvghad, *Corros. Sci.*, **107**, 133–144 (2016).
37. W. Hu and E. I. Meletis, *Mater. Sci. Forum*, **331**–**337**, 1683–1688 (2000).
38. J. B. Lumsden, M. W. Mahoney, G. Pollock, and C. G. Rhodes, *Corrosion*, **55**, 1127–1135.
39. M. J. Robinson and N. C. Jackson, *Corros. Sci.*, **41**, 1013–1028 (1999).
40. M. J. ROBINSON, *Corros. Sci.*, **23**, 887–899 (1983).
41. C. Gao, Z. Zhu, J. Han, and H. Li, *Mater. Sci. Eng. A*, **639**, 489–499 (2015).
42. W. Zhang and G. S. Frankel, *Electrochim. Acta*, **48**, 1193–1210 (2003).
43. X. Zhou, C. Luo, T. Hashimoto, A. E. Hughes, and G. E. Thompson, *Corros. Sci.*, **58**, 299–306 (2012).
44. A. E. Hughes et al., in *Recent Trends in Processing and Degradation of Aluminium Alloys*,, p. 223–262, InTech (2011)..
45. C. Luo, X. Zhou, G. E. Thompson, and A. E. Hughes, *Corros. Sci.*, **61**, 35–44 (2012).
46. T. M. D. C. Kumai, J. Kusinski, G. Thomas, *Corros. Sci.*, 294–302 (1989).
47. J. F. Li, Z. Q. Zheng, N. Jiang, and S. C. Li, *Mater. Corros.*, **56**, 192–196 (2005).
48. X. Y. Liu et al., *J. Alloys Compd.*, **639**, 263–267 (2015).
49. J. E. Kertz, P. I. Gouma, and R. G. Buchheit, *Metall. Mater. Trans. A*, **32**, 2561–2573 (2001).
50. A. Steuwer et al., *Acta Mater.*, **59**, 3002–3011 (2011).
51. H. Qin, H. Zhang, and H. Wu, *Mater. Sci. Eng. A*, **626**, 322–329 (2015).
52. M. J. Starink, A. J. Hobson, and P. J. Gregson, *Scr. Mater.*, **34**, 1711–1716 (1996).
53. P. S. Chen and B. N. Bhat, *Tech. Rep.* (2002).
54. M. X. Milagre et al., *Mater. Charact.*, **140**, 233–246 (2018).